# Image Restoration under Mixed Noise Using Globally Convex Segmentation

Jun Liu, Zhongdan Huan, Haiyang Huang\*

School of Mathematical Sciences, Beijing Normal University, Laboratory of Mathematics and Complex Systems, Ministry of Education, Beijing, 100875, P.R. China.

#### Abstract

The total variation based regularization method has been proven to be quite efficient for image restoration. However, the noise in the image is assumed to be Gaussian in the overwhelming majority of researches. In this paper, an extended ROF model is presented to restore image with non-Gaussian noise, in which the locations of the blurred pixels with high level noise are detected by a function and two estimated parameters of noise, while the fidelity and smoothness terms can be adaptively adjusted by updating these parameters. In contrast to the previous method, our model can give a much better restoration in some particular cases, such as the blurred image corrupted by impulsive noise and mixed noise. Moreover, the proposed minimization problem is solved by the split Bregman iteration, which makes our algorithm very fast. We provide some experiments and comparisons with other methods to illustrate the high efficiency of our method.

## Key words:

Total variation, Globally convex segmentation, Split Bregman iteration, Mixed noise, Impulsive noise.

#### 1. Introduction

Image deblurring, as a form of image restoration which is to recover latent clear images from degraded ones, is well developed. But it still attract attentions of so many researchers for it plays a active role in so many applications

Preprint submitted to Journal of Visual Communication and Image Representation April 3, 2010

<sup>\*</sup>The corresponding author, email address: hyhuangbnu@gmail.com

and the corresponding ill-posed inverse problem. Mathematically, the image degraded process can be modeled by

$$g = k * f + n$$

where  $g: \Omega \to [0,1]$  is the observed image, f represents the original image, n denotes noise, k usually stands for a known space invariant blur kernel and the symbol "\*" refers to the convolution operator.

Total variation (TV) based regularization technique was first introduced in computer vision by Rudin, Osher and Fatemi [1]. It has been proved to be quite efficient for regularizing images due to its good edge-preserving property. The famous TV-based image deblurring model, namely the ROF model, could be described as

$$f^* = \operatorname*{arg\,min}_f \frac{\mu}{2} ||k*f - g||_2^2 + \int_{\Omega} |\nabla f|.$$

Here  $\mu > 0$  is a scale parameter, the first term is a  $L^2$ -based fidelity term which can deblur the image, and the second is the TV smoothness term which can suppress noise. Many numerical experiments (e.g. [1, 2, 3, 4]) have shown its efficiency under a small amount of Gaussian noise. However, in many real world applications, noise in the image is often non-Gaussian, such as impulsive noise, Gaussian noise plus impulsive noise, mixed Gaussian noise, and so on. In these cases, reconstructions with ROF model are usually not satisfactory.

In recent years, some variational methods of recovering images corrupted by non-Gaussian noise have been explored. Nikolova  $et\ al.\ [5,\ 6]$  proposed some nonsmooth fidelity terms such as  $L^1$ -based fidelity terms to remove impulsive noise using variational regularization method, and Bar  $et\ al.\ [7]$  developed it by considering different Mumford-Shah (MS) functional regularization. In  $[8,\ 9]$ , Cai  $et\ al.\$ introduced a two-phase method to deblur images with both Gaussian noise and impulsive noise together, the main idea of their method is that using median-type filters to identify the possible noisy pixels and then employing the MS segmentation functional based variational method to restore image. To be slightly different from [8], Huang  $et\ al.\ [10]$  used TV regularization and  $L^2$  norm based fidelity term to reconstruct the image, and then they offered a fast alternating minimization algorithm. Our previous work [11] studied image restoration under mixed Gaussian noise by TV-based maximum penalized likelihood estimation (MPLE) and the

expectation-maximization (EM) algorithm. Compared with ROF model, all of these approaches have their own superiorities in some certain special cases.

Other than the existing methods, in this paper, we discuss a new approach that restoring images contaminated by mixed noise using globally convex segmentation method and TV regularization. This note is related to [11], and the key point is that, in each pixel, denoising and deblurring could be automatically adjusted according to the estimated information of noise. To be different from [11], we give a new model and a new algorithm in this study, which has a slightly better restoration and requires much less computational time.

The outline of the rest paper is as follows: In Section 2, the proposed theoretical model is presented. We describe how to solve the proposed minimization problem by split Bregman iteration in Section 3, and our experimental results are shown in Section 4. Finally, some conclusions and discussions about this paper are given in section 5.

#### 2. The Theoretical Model

In [11], the authors assume the intensity of noise n(x) is a random variable at each point x, and all these random variables  $\{n(x):x\in\Omega\}$  are independent and identically-distributed with a Gaussian mixture model. Then using the TV-based MPLE for noise and EM algorithm, a minimization problem is introduced to restore the blurred image in the presence of mixed noise:

$$(f^*,\alpha_1^*,\alpha_2^*,(\sigma_1^2)^*,(\sigma_2^2)^*) = \underset{f,\alpha_1,\alpha_2,\sigma_1^2,\sigma_2^2}{\arg\min} E(f,\alpha_1,\alpha_2,\sigma_1^2,\sigma_2^2).$$

Where

$$E(f, \alpha_1, \alpha_2, \sigma_1^2, \sigma_2^2) = \lambda_1 \int_{\Omega} |\nabla f| \, dx + \sum_{l=1}^2 \int_{\Omega} \alpha_l dx + \frac{1}{2} \sum_{l=1}^2 \int_{\Omega} \omega_l^{\nu}(x) \ln \sigma_l^2 dx - \sum_{l=1}^2 \int_{\Omega} \omega_l^{\nu}(x) \ln \alpha_l dx + \frac{1}{2} \sum_{l=1}^2 \int_{\Omega} \frac{[(k * f)(x) - g(x)]^2}{\sigma_l^2} \omega_l^{\nu}(x) dx,$$

 $\alpha_1,\alpha_2,\sigma_1^2,\sigma_2^2$  are four unknown variables , and

$$\omega_l^{\nu}(x) = \frac{\alpha_l^{\nu} p_l((k * f^{\nu})(x) - g(x); (\sigma_l^2)^{\nu})}{\sum_{c=1}^2 \alpha_c^{\nu} p_c((k * f^{\nu})(x) - g(x); (\sigma_c^2)^{\nu})}$$

is a known weighting function for given the  $\nu$ -th iterative values of  $f, \alpha_l$  and  $\sigma_l^2$ , here  $p_l$  is the Gaussian density function parameterized by  $(\sigma_l^2)^{\nu}$ . More details about this model can be found in [11].

The above model, in fact, is an extension of ROF model, since if the variables are all fixed constants such that  $\alpha_1 = \alpha_2$ ,  $\sigma_1^2 = \sigma_2^2$ , it would be reduced to the ROF model. We observe that  $\sum_{l=1}^2 \omega_l^{\nu}(x) = 1$ , and  $\omega_l^{\nu}(x)$  plays a role of the characteristic function of a certain area. Therefore, ignoring  $\alpha_l$  and adding a constraint on the length of borderline curve of the area, the above functional could be approximated by level set representations [12] as follows:

$$\begin{split} E(f,\phi,\sigma_{1}^{2},\sigma_{2}^{2}) &= \lambda_{1} \int_{\Omega} |\nabla f| + \lambda_{2} \int_{\Omega} |\nabla H(\phi)| \\ &+ \frac{1}{2} \int_{\Omega} H(\phi) \ln \sigma_{1}^{2} + \frac{1}{2} \int_{\Omega} (1 - H(\phi)) \ln \sigma_{2}^{2} \\ &+ \frac{1}{2} \int_{\Omega} \frac{(k * f - g)^{2}}{\sigma_{1}^{2}} H(\phi) + \frac{1}{2} \int_{\Omega} \frac{(k * f - g)^{2}}{\sigma_{2}^{2}} (1 - H(\phi)). \end{split}$$

Where  $\lambda_1 > 0$ ,  $\lambda_2 > 0$  are both regularization parameters, and  $\phi, H$  denote the level set and Heaviside functions, respectively.

The cost functional E is non-convex respect to  $\phi$  and may have local minima. Recently, some globally convex segmentation (GCS) methods which are very reliable have been proposed by Chan *et al.* [13] and Bresson *et al.* [14]. By applying the GCS framework, our new model can be expressed as

$$(f^*, u^*, (\sigma_1^2)^*, (\sigma_2^2)^*) = \underset{f, \ 0 \le u \le 1, \ \sigma_1^2, \ \sigma_2^2}{\arg \min} E(f, u, \sigma_1^2, \sigma_2^2), \tag{1}$$

and

$$E(f, u, \sigma_1^2, \sigma_2^2) = \frac{1}{2} \int_{\Omega} u \ln \sigma_1^2 + \frac{1}{2} \int_{\Omega} (1 - u) \ln \sigma_2^2 + \frac{1}{2} \int_{\Omega} (\frac{u}{\sigma_1^2} + \frac{1 - u}{\sigma_2^2}) (k * f - g)^2 + \lambda_1 \int_{\Omega} |\nabla f| + \lambda_2 \int_{\Omega} |\nabla u|.$$

We claim that this model has a better performance than others in suppressing mixed noise. Some intuitionistic interpretations are given in the following paragraph.

Let us emphasize again that the ROF model is a special case of the proposed method with  $\sigma_1^2 = \sigma_2^2$ , and  $\lambda_2 = 0$ . In order to better explain the

superiority of our approach, let us consider a particular type of mixed noise impulse noise. When a blurred image corrupted by impulse noise, where only a portion of the blurred pixels are contaminated by noise, in such case, the image domain  $\Omega$  can be divided into two nonoverlapping parts  $\Omega_1$  and  $\Omega_2$ , one of which  $(\Omega_1)$  contains the pixels only with blur and the other  $(\Omega_2)$  contains high level noise. On the other hand, if we solve (1) iteratively with alternating minimization algorithm, the discussed image restoration problem would split into three steps: noise image segmentation, parameter adjustment, and image restoration. Suppose  $f, \sigma_1^2, \sigma_2^2$  are known, minimizing E with respect to u is an image segmentation problem, however, it is different from the traditional image segmentation in which the pixels are usually clustered by different means, and here the pixels of the estimated noise image are classified according to different variances. The model (1) is originally derived from EM algorithm (cf. [11]), and it is well known that the segmentation results with EM algorithm partly depend on the initial parameter values since the EM algorithm only has local convergence. The GCS method do not depend on the initial guess value and has a better performance in image segmentation (cf. [14]). Applying the GCS segmentation, we hope  $u(x) = \chi_{\Omega_1}(x)$ , where  $\chi$  is a characteristic function. Once the idealized u, f are known, minimizing E with respect to  $\sigma_1^2$ , and  $\sigma_2^2$  leads to  $\sigma_1^2 = \int_{\Omega_1} (k*f-g)^2/|\Omega_1|$  and  $\sigma_2^2 = \int_{\Omega_2} (k * f - g)^2 / |\Omega_2|$ , respectively, where  $|\cdot|$  denotes the area. Thus in the image restoration step, the fidelity term (corresponding to the third term) in the cost functional E equals to  $\frac{|\Omega_1|}{2} + \frac{|\Omega_2|}{2} = \frac{|\Omega|}{2}$ . That is, the value of fidelity term in our model is almost a constant for any levels of noise. However, the total variation of the image in  $\Omega_2$  is always larger than that in  $\Omega_1$  due to heavy noise exists in  $\Omega_2$ . As we expect, the smoothness term in cost functional will play a greater role in  $\Omega_2$  than  $\Omega_1$  when minimizing E. In other word, the local behaviors of denoising and deblurring can be adaptively adjusted by  $u, \sigma_1^2$ , and  $\sigma_2^2$  though a fixed global regularization term is utilized in our model, this is much different from the existing method such as ROF model.

The objective functional E is convex with respect to f and u, respectively. However, it is only conditionally convex with respect to  $\sigma_1^2$  and  $\sigma_2^2$  provided that

$$0 < \sigma_1^2 \leqslant \frac{2\int_{\Omega} (k*f - g)^2 u}{\int_{\Omega} u}, \ 0 < \sigma_2^2 \leqslant \frac{2\int_{\Omega} (k*f - g)^2 (1 - u)}{\int_{\Omega} (1 - u)}.$$

Now, let us introduce two variables  $z_1, z_2$  such that  $z_1 = \ln \sigma_1^2, z_2 = \ln \sigma_2^2$ ,

then (1) becomes

$$\min_{\substack{f,0 \leq u \leq 1, z_1, z_2 \\ d}} \left\{ E(f, u, z_1, z_2) = \frac{1}{2} \int_{\Omega} u z_1 + \frac{1}{2} \int_{\Omega} (1 - u) z_2 + \frac{1}{2} \int_{\Omega} [u e^{-z_1} + (1 - u) e^{-z_2}] (k * f - g)^2 + \lambda_1 \int_{\Omega} |\nabla f| + \lambda_2 \int_{\Omega} |\nabla u| \right\}$$

As a result, the above E is convex with respect to  $z_1$  and  $z_2$ , respectively. We make the cost functional is convex with respect to each variable because that the convexity ensures the alternating minimization (AM) algorithm can be used to solve (2). We will discuss the algorithms in the next.

## 3. Algorithms

In this section, we present an efficient algorithm for minimization problem (2). For convenience, let us denote

$$H(f, u, z_1, z_2) = \int_{\Omega} u z_1 + \int_{\Omega} (1 - u) z_2 + \int_{\Omega} [u e^{-z_1} + (1 - u) e^{-z_2}] (k * f - g)^2.$$

First, the AM algorithm splits (2) into three subproblems: Subproblem 1,

$$f^{\nu+1} = \underset{f}{\arg\min} \left\{ \frac{1}{2} H(f, u^{\nu}, z_1^{\nu}, z_2^{\nu}) + \lambda_1 \int_{\Omega} |\nabla f| \right\}.$$

Subproblem 2,

$$u^{\nu+1} = \operatorname*{arg\,min}_{0 \leqslant u \leqslant 1} \left\{ \frac{1}{2} H(u, f^{\nu+1}, z_1^{\nu}, z_2^{\nu}) + \lambda_2 \int_{\Omega} |\nabla u| \right\}.$$

Subproblem 3,

$$(z_1^{\nu+1}, z_2^{\nu+1}) = \underset{z_1, z_2}{\operatorname{arg \, min}} \left\{ \frac{1}{2} H(u^{\nu+1}, f^{\nu+1}, z_1, z_2) \right\}.$$

There are many methods could be used to solve subproblems 1 and 2, such as the steepest descent method [1], fixed point iteration [3, 4], dual method [15, 16], augmented Lagrangian method [17], split Bregman iteration [18],

and so on. Considering the high efficiency and robustness of split Bregman iteration, we will apply it to solve these subproblems.

The split Bregman methods [18] is a general  $L^1$  minimization technique. To apply the split Bregman iteration to subproblem 1, we add the auxiliary variable  $\mathbf{d}_1^{\nu+1}$  and the Bregman vector  $\mathbf{b}_1^{\nu}$  to the functional. Then we solve a sequence of unconstrained problems defined by

$$\begin{cases}
(f^{\nu+1}, \mathbf{d}_{1}^{\nu+1}) &= \underset{f, \mathbf{d}_{1}}{\arg\min \frac{1}{2}} H(f) + \lambda_{1} \int |\mathbf{d}_{1}| + \frac{\mu_{1}}{2} \int |\mathbf{d}_{1} - \nabla f - \mathbf{b}_{1}^{\nu}|^{2}, \\
\mathbf{b}_{1}^{\nu+1} &= \mathbf{b}_{1}^{\nu} + \nabla f^{\nu+1} - \mathbf{d}_{1}^{\nu+1}.
\end{cases} (3)$$

Similarly, the split Bregman formulas of subproblem 2 are given by

$$\begin{cases}
(u^{\nu+1}, \mathbf{d}_{2}^{\nu+1}) &= \underset{0 \leq u \leq 1, \mathbf{d}_{2}}{\arg \min \frac{1}{2}} H(u) + \lambda_{2} \int |\mathbf{d}_{2}| + \frac{\mu_{2}}{2} \int |\mathbf{d}_{2} - \nabla u - \mathbf{b}_{2}^{\nu}|^{2}, \\
\mathbf{b}_{2}^{\nu+1} &= \mathbf{b}_{2}^{\nu} + \nabla u^{\nu+1} - \mathbf{d}_{2}^{\nu+1}.
\end{cases} (4)$$

Here  $\mu_1 > 0$  and  $\mu_2 > 0$  are both parameters. More details and theoretical results about this algorithm, please see references [18, 19].

The alternating minimization scheme is again employed for (3). Let us denote  $\omega^{\nu} = u^{\nu}e^{-z_1^{\nu}} + (1 - u^{\nu})e^{-z_2^{\nu}}$ , then  $f^{\nu+1}$  in (3) is obtained by solving the Euler-Lagrange equation

$$\hat{k} * [\omega^{\nu}(k * f)] - \mu_1 \triangle f = \hat{k} * (\omega^{\nu} g) + \mu_1 \operatorname{div}(\mathbf{b}_1^{\nu} - \mathbf{d}_1^{\nu}),$$
 (5)

which is a linear equation and easy to solve by the conjugate gradient (CG) method. Here  $\hat{k}$  is the conjugated function of k.

It is not difficult to show that minimization with respect to  $\mathbf{d_1}$  in (3) can be done explicitly by

$$\mathbf{d}_1^{\nu+1} = \operatorname{shrink}(\nabla f^{\nu+1} + \mathbf{b}_1^{\nu}, \frac{\lambda_1}{\mu_1}),$$

where shrink is an operator which has an expression

$$shrink(\mathbf{y}, \lambda) = \frac{\mathbf{y}}{|\mathbf{y}|} \max\{|\mathbf{y}| - \lambda, 0\}.$$

Next, let us define  $r = z_1^{\nu} - z_2^{\nu} + (e^{-z_1^{\nu}} - e^{-z_2^{\nu}})(k * f^{\nu+1} - g)^2$ , then the Euler-Lagrange equation of (4) with respect to u is given by

$$-\Delta u = \operatorname{div}(\mathbf{b}_2^{\nu} - \mathbf{d}_2^{\nu}) - \frac{r}{2\mu_2}, \text{ whenever } 0 < u < 1,$$

and we choose the fast Gauss-Seidel (GS) method to approximately solve this system. Considering the constraint  $0 \le u \le 1$  and then following [19], a closed-form iteration scheme can be written by

$$\alpha_{i,j} = \left[\operatorname{div}(\mathbf{b}_2^{\nu} - \mathbf{d}_2^{\nu}) - \frac{r}{2\mu_2}\right]_{i,j},$$

$$\beta_{i,j} = \frac{1}{4} (u_{i+1,j}^{\nu_1} + u_{i-1,j}^{\nu_1} + u_{i,j+1}^{\nu_1} + u_{i,j-1}^{\nu_1} + \alpha_{i,j}), \tag{6}$$

$$u_{i,j}^{\nu_1+1} = \max\{\min\{\beta_{i,j}, 1\}, 0\}, \tag{7}$$

where  $\nu_1$  is the number of the GS inner iteration. As has been stated earlier,  $\mathbf{d}_{2}^{\nu+1}$  has the form

$$\mathbf{d}_2^{\nu+1} = \operatorname{shrink}(\nabla u^{\nu+1} + \mathbf{b}_2^{\nu}, \frac{\lambda_2}{\mu_2}).$$

Finally, we need to solve subproblem 3. It is easy to calculate the optimality criteria for  $z_1^{\nu+1}$  and  $z_2^{\nu+1}$  are given by

$$z_1^{\nu+1} = \ln \frac{\int_{\Omega} u^{\nu+1} (k * f^{\nu+1} - g)^2}{\int_{\Omega} u^{\nu+1}},$$
 (8)

$$z_2^{\nu+1} = \ln \frac{\int_{\Omega} (1 - u^{\nu+1})(k * f^{\nu+1} - g)^2}{\int_{\Omega} (1 - u^{\nu+1})}.$$
 (9)

As a result, the implementation of our model can be summarized as follows:

**Algorithm** Split Bregman iteration for the model (2)

Choose initial values  $f^0 = g, u^0 = 1, z_1^0 = \ln(10^{-4}), z_2^0 = \ln 1.0 = 0, \mathbf{b}_1^0 = 0$  $\mathbf{b}_{2}^{0} = \mathbf{d}_{1}^{0} = \mathbf{d}_{2}^{0} = \mathbf{0}$ , set  $\nu = 0$ , and do:

- 1. Compute  $f^{\nu+1}$  by (5) using a CG solver, and we refer to this step as the CG inner iteration;
- CG inner iteration; 2. If  $||f^{\nu+1} f^{\nu}||_{\infty} < 10^{-3}$ , end the algorithm. Else, go to the next step; 3.  $\mathbf{d}_{1}^{\nu+1} = \operatorname{shrink}(\nabla f^{\nu+1} + \mathbf{b}_{1}^{\nu}, \frac{\lambda_{1}}{\mu_{1}});$ 4.  $\mathbf{b}_{1}^{\nu+1} = \mathbf{b}_{1}^{\nu} + \nabla f^{\nu+1} \mathbf{d}_{1}^{\nu+1};$ 5. Find  $u^{\nu+1}$  by GS inner iteration, i.e. calculating (6) and (7) repeatedly; 6.  $\mathbf{d}_{2}^{\nu+1} = \operatorname{shrink}(\nabla u^{\nu+1} + \mathbf{b}_{2}^{\nu}, \frac{\lambda_{2}}{\mu_{2}});$ 7.  $\mathbf{b}_{2}^{\nu+1} = \mathbf{b}_{2}^{\nu} + \nabla u^{\nu+1} \mathbf{d}_{2}^{\nu+1};$ 8. Update  $z_{1}^{\nu+1}, z_{2}^{\nu+1}$  by (8) and (9), respectively;

- 9.  $\nu = \nu + 1$ , go to 1.



Figure 1: The original image I for the experiments.

## 4. Experimental Results

We present some numerical results of the proposed model in this section. First of all, let us discuss how to choose the parameters which occur in our algorithm. The experimental experiences tell us that the parameter values are not needed to change according to the levels of noise. This stems from the fact that the performances of denoising and deblurring can be adaptively balanced by updating parameters  $z_1$  and  $z_2$  (recalling that  $e^{z_1} = \sigma_1^2, e^{z_2} = \sigma_2^2$  are two parameters of the variance of noise). So, in all the following experiments, we set  $\lambda_1 = 5, \mu_1 = 10\lambda_1, \lambda_2 = 10^{-3}, \mu_2 = 10\lambda_2, z_1^0 = \ln(0.05)$  for random-valued noise and  $z_1^0 = \ln(10^{-4})$  for other noise. Beyond that, the CG inner iteration is ended when  $||f^{\nu_1+1} - f^{\nu_1}||_{\infty} < 10^{-3}$ , where  $\nu_1$  is the number of the CG iteration, and the iteration number of GS inner iteration in the algorithm is set to 5.

The peak signal to noise ratio PSNR =  $10 \log_{10} \frac{M \times N}{||f-I||_2^2}$  is taken to measure the efficiency of our approach, where  $M \times N$  is the image size, f represents the restoration, and I stands for the original image. The clear original images with size  $256 \times 256$  are shown in Figure 1.

Recently, an efficient algorithm called FTVd for ROF and TVL<sup>1</sup> problem

$$\min_{f} \int_{\Omega} |\nabla f| + \mu ||f - g||_{1}$$

was proposed in [20, 21]. So, we use their code which can be downloaded freely from the internet for comparing different models with ours. In addition, we will compare the presented method with some state of the art deblurring algorithms such as SA-DCT in [22] and BM3DDEB in [23]. As is well know, parameters are very important for such models (e.g.  $\mu$  in ROF, TVL<sup>1</sup>) to obtain a good reconstruction, thus in the following experiments, for each

algorithm, we test different parameters values and choose the restoration with the highest PSNR for the comparison.

Table 1: PSNR (dB) values and CPU time (s) in the experiment 1.

	Deconvwnr	Deconvreg	ROF	[22]	[23]	[11]	proposed
PSNR	20.91	22.31	22.91	22.98	23.52	25.03	24.95
CPU time	0.08	0.57	2.52	6.28	6.50	53.41	14.33

## 4.1. Experiment 1, suppressing Gaussian mixed noise.

A comparison of the reconstructions obtained by Wiener filter, iterative regularization technique, the ROF model, SA-DCT in [22], BM3DDEB in [23], the method in [11], and the proposed algorithm is shown in Figure 2. The Lenna image is blurred by an out-of-focus blur with radius 5, then is corrupted by two Gaussian noise with different variances ( $\sigma_1^2 = 2 \times 10^{-4}, \sigma_2^2 =$  $2 \times 10^{-2}$ ), and the mixing ratio is 3:1, see Figure 2(a). The reconstructions with these seven algorithms are shown in Figure 2(b)-Figure 2(h), respectively. Figure 2(i) is  $q \cdot u$ , the estimated image with low level noise, in which the non-zero values should be the pixels with low level noise. It can be seen that the proposed method produces much better result than other methods, and has similar visual effects to [11]. However, it requires much less cpu time than [11]'s. The corresponding PSNR values and the cpu time are summarized in Table 1. The above experiment shows that our algorithm produces better result than SA-DCT and BM3DDEB methods under Gaussian mixed noise, however, one can incorporate our idea with SA-DCT or BM3DDEB methods to get better results.

## 4.2. Experiment 2, suppressing salt-and-pepper noise.

The model (2) is especially suitable for deblurring image under impulsive noise such as salt-and-pepper noise and random-valued noise, this is because of the fact that a certain number of pixels in a image which is contaminated by impulse noise are uncorrupted. Our method can automatically find them by u and give a good restoration, especially for high level noise.

For salt-and-pepper noise, the corrupted pixels have minimal intensities 0 or maximal intensities 1. Thus, according to this prior knowledge, the initial



Figure 2: Comparison: (a) blurred (out-of-focus blur, radius=5) image with mixed Gaussian noise( $\sigma_1^2=2\times 10^{-4},\sigma_2^2=2\times 10^{-2}$ ). (b) restored by Wiener filter with Matlab function "deconvent". (c) restored by iterative regularization technique with Matlab function "deconvreg".(d) restored by ROF,  $\mu=150$ . (e) restored by SA-DCT in [22], parameters  $\varepsilon_1=0.65, \varepsilon_2=0.002$ . (f) restored by BM3DDEB in [23], parameters  $\varepsilon_{RI}=0.0001, \varepsilon_{RWI}=0.001$ . (g) restored by the method in [11]. (h) restored by the proposed method. (i) the estimated image with low level noise in the proposed approach, that is,  $g\cdot u$ .

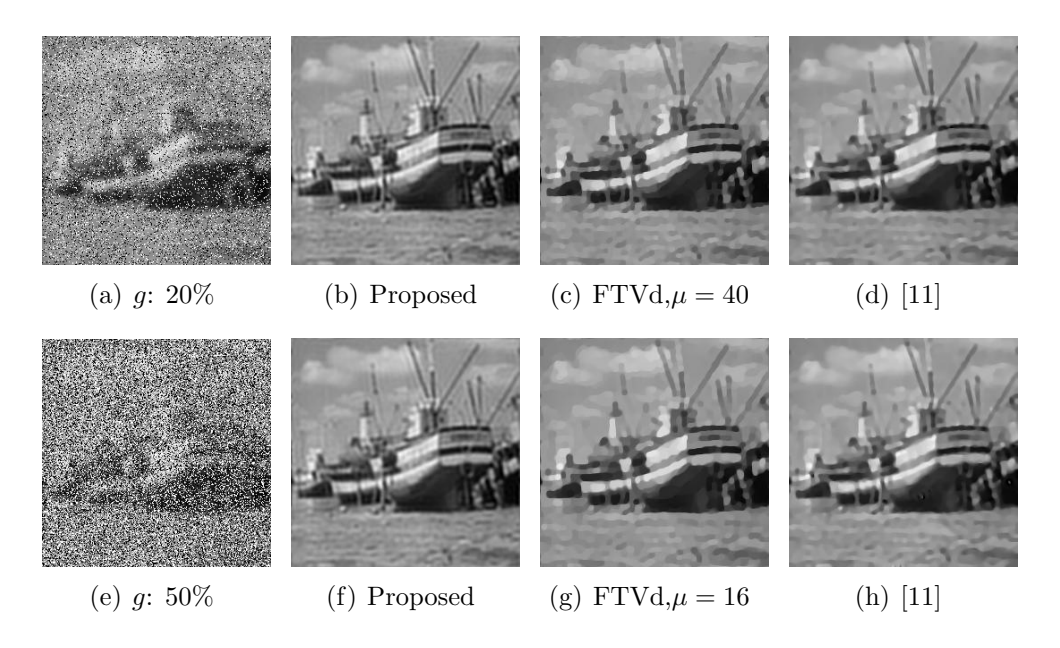


Figure 3: Recovering blurred (Gaussian blur,  $\sigma=3.0$ ) images with salt-and-pepper noise using different methods. First column: from top to bottom 20%, 50% salt-and-pepper noise. Second, third, fourth column: reconstructions with the proposed method,  $\text{TVL}^1$ , and method in [11], respectively.

Table 2: PSNR (dB) values and CPU time (s) in the experiment 2.

	PSNR	(dB)		CPU	$_{ m time}$	(s)
Noise level	[11]	$\mathrm{TVL}^1$	proposed	[11]	$\mathrm{TVL}^1$	proposed
20%	26.13	25.30	26.32	95.43	6.63	3.70
50%	25.96	25.06	26.27	187.05	7.19	4.12
80%	-	22.19	26.11	-	5.88	4.62
95%	-	14.94	24.29	-	13.48	5.60

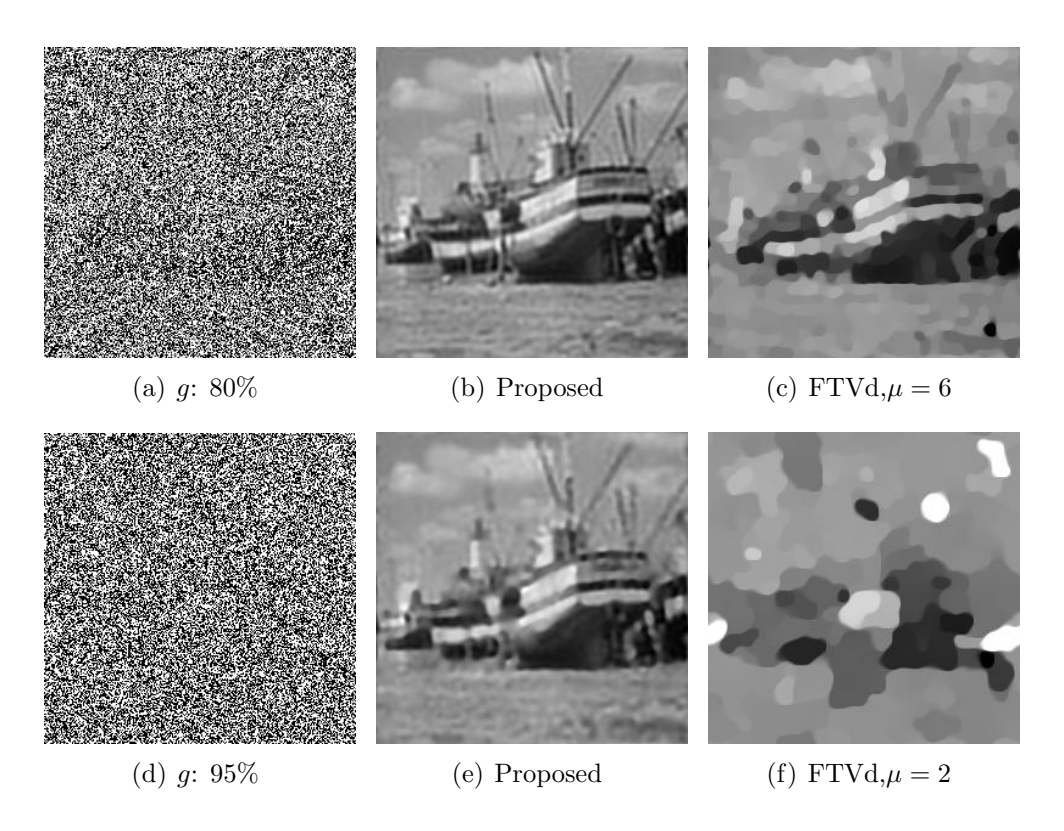


Figure 4: Recovering blurred (Gaussian blur,  $\sigma=3.0$ ) images with high levels salt-and-pepper noise. (a),(d): 80%, 95% salt-and-pepper noise. (b),(e): reconstructions with the proposed method. (c),(f): reconstructions with TVL<sup>1</sup>.

 $u^0$  in our algorithm can be set

$$u^{0}(x) = \begin{cases} 1 & g(x) \neq 0 \text{ or } 1, \\ 0 & g(x) = 0 \text{ or } 1. \end{cases}$$

Figure 3 shows some results by applying the methods in this paper, in [11] and TVL¹ model, which is designed to restore image with impulsive noise [5, 7, 21]. The images in the first column of Figure 3 are the contaminated Boat image with Gaussian blur (standard deviation=3.0) and different levels of salt-and-pepper noise, the densities of salt-and-pepper noise are 20%, 50%, respectively, and the corresponding restorations with different methods can be found in the last three columns. The corresponding PSNR values and the cpu time can be found in Table 2.

We find that our model can still work even though 80 or 95 percent of the blurred pixels are corrupted by salt-and-pepper noise, because this kind of noise is easy to detect. The results of restoring blurred image with such high level noise are illustrated in Figure 4. One can find that the proposed method gives much better restorations with higher PSNR values, and less cpu time (see Table 2) than TVL<sup>1</sup>, especially the levels of noise are high.

Table 9. I state (ab) varies and CI c time (b) in the experiment 9.							
Noise	PSNR	(dB)		CPU	$_{ m time}$	(s)	
ratio	$\mathrm{TVL}^1$	Two-phase	proposed	$TVL^1$	Two-phase	proposed	
55%	24.12	25.98	27.13	4.25	184.27	10.83	
70%	20.78	23.01	24.72	8.45	211.65	11.10	

Table 3: PSNR (dB) values and CPU time (s) in the experiment 3

#### 4.3. Experiment 3, suppressing random-valued noise.

Another common type of impulse noise is random-valued noise, in this case, the changed pixels in a blurred image are some random numbers with a uniform distribution in [0,1].

Recently, In [8, 9], a two-phase method is proposed to deblur image under impulse noise and it can provide good results. The two-phase method can be described as minimizing the following functional

$$\int_{\Omega} \chi \cdot |k * f - g| + \beta R(f),$$

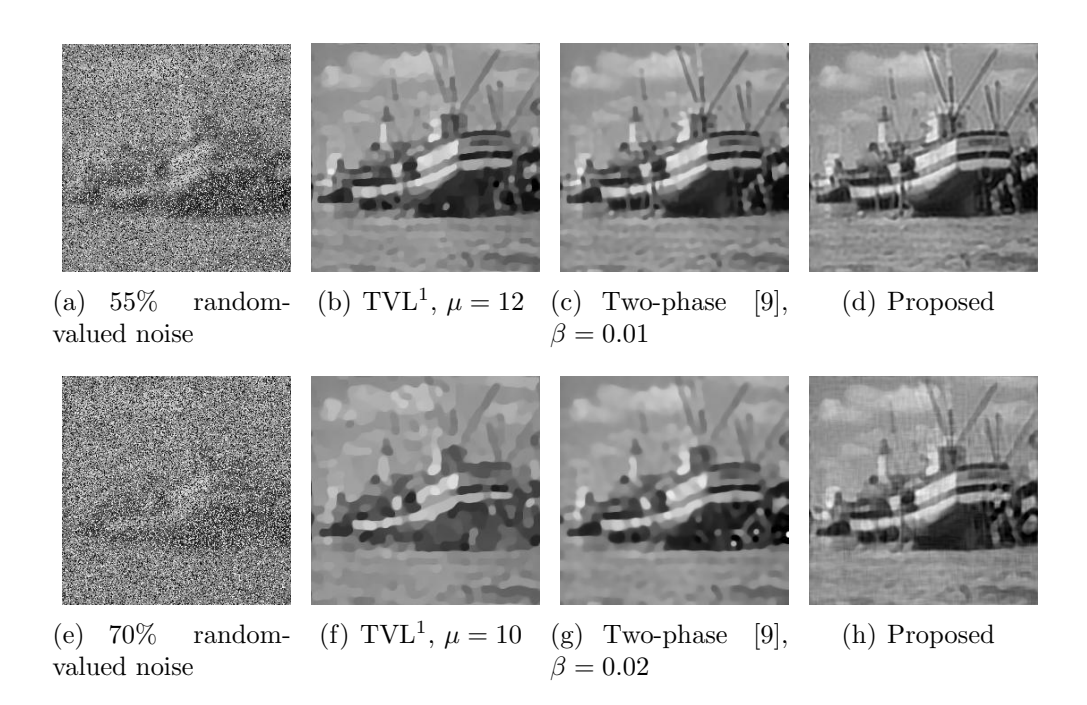


Figure 5: Recovering blurred images with random-valued noise: (a),(e) blurred image with random-valued noise. (b),(f) restored by TVL<sup>1</sup>. (c),(g) restored by the two-phase method [9]. (d),(h) restored by the proposed method.

where  $\beta > 0$  is a parameter, R(f) is a regularization term, and  $\chi$  is a characteristic function which is estimated by median-type filter in the two-phase method.  $\chi$  is determined by formula

$$\chi(x) = \begin{cases} 1, & g(x) \text{ is a noise free pixel,} \\ 0, & g(x) \text{ is a likely noisy pixel.} \end{cases}$$

In general, it is more difficult to detect random-valued noise than salt-and-pepper noise. As is reported in [8, 9], the two-phase method can not give good restoration under random-valued noise with density more than 55% since there is no good median-type detector for random-valued noise when the noise ratio is high. However, the proposed model can work well in the presence of random-valued noise with density as high as 75%, because the noise detection and image restoration are implemented iteratively in the presented algorithm and the random-valued noise can be better identified. In Figure 5, we show the restorations with TVL<sup>1</sup>, the two-phase method [9], and model (2) under high level random-valued noise. In Figure 5(a), the original image is blurred

by a Gaussian blur with standard deviation  $\sigma = 3.0$ , and then is corrupted by random-valued noise with density 55%. While in Figure 5(e), the image is contaminated by a Gaussian blur with  $\sigma = 4.0$  and the noise ratio is 70%. The restorations of both cases with three algorithms are illustrated in the last three columns of Figure 5, respectively. We can see from the figures that our method is again much better than others. As before, We summarized the PSNR values and CPU time in Table 3.

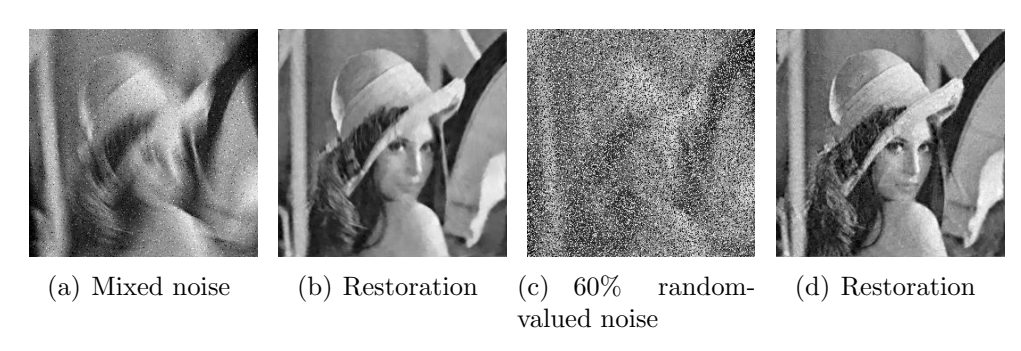


Figure 6: Recovering space-varying blurred images. (a) and (c) are the blurred images with Gaussian mixed noise ( $\sigma_1^2 = 10^{-4}, \sigma_2^2 = 2 \times 10^{-2}$ , the mixing ratio is 3:1), random-valued noise, respectively. (b) and (d) correspond to the restorations with the proposed method.

4.4. Experiment 4, recovering the images with space-varying blur and mixed noise.

In this experiment, we apply our algorithm to reconstruct the degraded images with space-varying blur. A very general model for the blurring of images is

$$g(x_1, x_2) = \int \int_{\Omega} k(x_1, x_2, y_1, y_2) f(y_1, y_2) dy_1 dy_2 + n(x_1, x_2).$$

We consider the known blur kernel has the expression

$$k(x_1, x_2, y_1, y_2) = \begin{cases} \frac{1}{2L(x_1, x_2)}, & y_1^2 + y_2^2 \leqslant L^2(x_1, x_2) \\ & \text{and } y_1 sin\theta(x_1, x_2) - y_2 cos\theta(x_1, x_2) = 0, \\ 0, & \text{else,} \end{cases}$$

where

$$L(x_1, x_2) = \frac{9}{255}x_2 + 6,$$
  

$$\theta(x_1, x_2) = \frac{\pi}{255}x_1 - \frac{\pi}{2}.$$

In the experiment, the image size is  $256 \times 256$ , while the coordinate has an origin at the upper left of the image.

Figure 6 illustrates the results of recovering the images with space-varying blur and Gaussian mixed noise/random-valued noise. One can find that our method still provides good restorations.

# 4.5. Experiment 5, Natural images reconstructing.

Figure 7 contains some results by applying our algorithm to real data, which was taken by surveillance cameras in the railway lines at nightfall. These images often have low contrast and noise. A result with histogram equalization is illustrated in Figure 7(b), we can see from the figure that noise is amplified. Figure 7(c), Figure 7(d) show the results with our method and ROF model, and one can find that noise is suppressed efficiently in both method. However, our method provides clearer details than ROF. Here, we set the blur kernel k to the Delta function for both methods.

#### 5. Conclusion and Discussion

In this note, we have proposed a new model to restore image from mixed noisy data. In our method, the classical cost functionals of image segmentation and image restoration are coupled together by introducing two extra terms, which are derived from the statistical process. A function u is employed to detect the locations of the possible noisy pixels, and a balance between denoising and deblurring can be found by updating the introduced paremeters  $z_1$  and  $z_2$ . All of these ensure that our approach has a better performance than others in removing mixed noise.

We mention that the method developed in this paper may be extended to blind convolution, inpainting, segmentation. Another possible extension is that employing some nonsmooth fidelity terms such as  $L^1$ -based fidelity terms in our model. Finally, we have not given the theoretical results of the proposed model, such as the existence and uniqueness of the regularized solution. These are future research contents.

# 6. Acknowledgements

We thank authors of [9, 20, 21, 22, 23] for their kind offer the Matlab source codes to make comparisons. we also thank the anonymous reviewers for their valuable comments. The research has been supported by National Science Foundation of China (NSFC, No. 10531040).

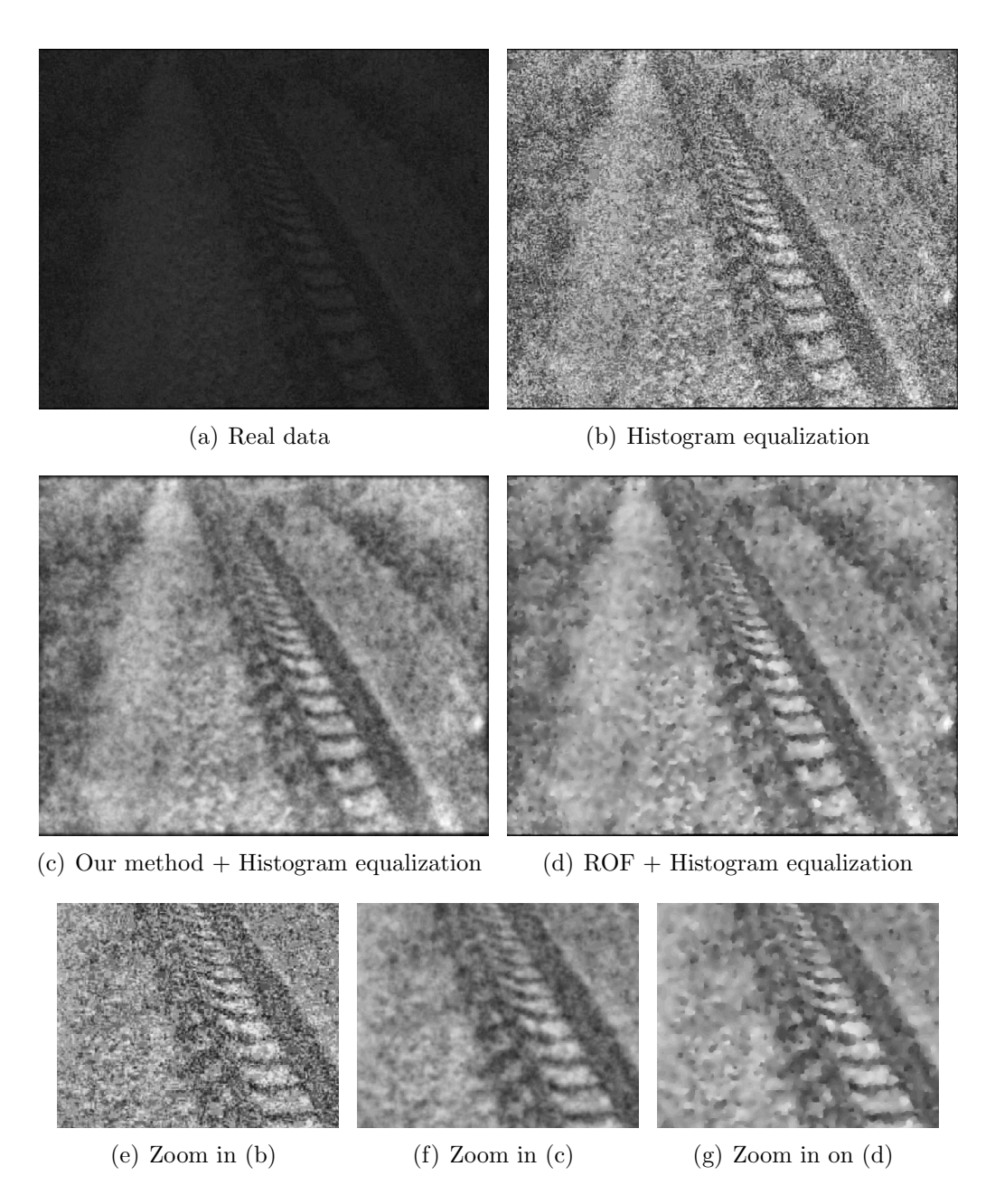


Figure 7: (a) Natural image. (b) result with histogram equalization. (c) reconstructing with our method, and then with histogram equalization. (d) reconstructing with ROF, and then with histogram equalization.

#### References

- [1] L. Rudin, S. Osher, and E. Fatemi, "Nonlinear total variation based noise removal algorithms," *Phys. D*, vol. 60, pp. 259-268, 1992.
- [2] L. Rudin, and S. Osher, "Total variation based image restoration with free local constraints," *IEEE ICIP 1994*, vol. 1, pp. 31-35, 1994.
- [3] C. Vogel, and M. Oman, "Iterative methods for total variation denoising," SIAM J. Sci. Comput., vol. 17, no. 1, pp. 227-238, Jan. 1996.
- [4] C. Vogel, and M. Oman, "Fast, robust total variation-based reconstruction of noisy, blurred images," *IEEE Trans. Image Process.*, vol. 7, no. 6, pp. 813-824, 1998.
- [5] M. Nikolova, "A variational approach to remove outliers and impulse noise," J. Math. Imag. Vis., vol. 20, pp. 99-120, 2004.
- [6] R. Chan, C. Ho, and M. Nikolova, "Salt-and-pepper noise removal by median-type noise detectors and edge-preserving regularization," *IEEE Trans. Image Process.*, vol. 14, no. 10, pp. 1479-1485, Oct. 2005.
- [7] L. Bar, N. Sochen, and N. Kiryati, "Image deblurring in the presence of impulsive noise," *Int. J. Comput. Vis.*, vol. 70, pp. 279-298, 2006.
- [8] J. Cai, R. Chan, and M. Nikolova, "Two-phase approach for deblurring images corrupted by impulse plus Gaussian noise," *Inv. Prob. Imag.*, Vol. 2, pp. 187-204, 2008.
- [9] J. Cai, R. Chan, and M. Nikolova, "Fast two-phase image deblurring under impulse noise," J. Math. Imaging Vis., DOI 10.1007/s10851-009-0169-7, 2009.
- [10] Y. Huang, M. Ng, and Y. Wen, "Fast image restoration methods for impulse and gaussian noises removal," *IEEE Sig. Process. Lett.*, Vol. 16, pp. 457-460, 2009.
- [11] J. Liu, Z. Huan, H. Huang, and H. Zhang, "An Adaptive Method for Recovering Image from Mixed Noisy Data," Int. J. Comput. Vis., vol. 85, no. 2, pp. 182-191, 2009.

- [12] T. Chan, and L. Vese, "Active contours without edges," *IEEE Trans. Image Process.*, vol. 10, pp. 266-277, 2001.
- [13] T. Chan, S. Esedoglu, and M. Nikolova. "Algorithms for finding global minimizers of image segmentation and denoising models." SIAM J. Appl. Math., vol. 66, pp. 1632-1648, 2006.
- [14] X. Bresson, S. Esedoglu, P. Vandergheynst, J. Thiran, and S. Osher, "Fast global minimization of the active contour/snake model," *J. Math. Imag. Vis.*, vol. 28, pp. 151-167, 2007.
- [15] T. Chan, G. Golub, and P. Mulet, "A nonlinear primal-dual method for total variation-based image restoration," SIAM J. Sci. Comput., vol. 20, pp. 1964-1977, 1999.
- [16] A. Chambolle, "An algorithm for total variation minimization and applications," J. Math. Imaging Vis., vol. 20, pp. 89-97, 2004.
- [17] X. Tai, and C. Wu, "Augmented Lagrangian method, dual methods and split Bregman iteration for ROF model," *UCLA CAM Report* 09-05, 2009.
- [18] T. Goldstein, and S. Osher, "The split Bregman method for L1 regularized problems," *UCLA CAM Report* 08-29, 2008.
- [19] T. Goldstein, X. Bresson, and S. Osher, "Geometric applications of the split Bregman method: segmentation and surface reconstruction," UCLA CAM Report 09-06, 2009.
- [20] Y. Wang, J. Yang, W. Yin, and Y. Zhang, "A new alternating minimization algorithm for total variation image reconstruction," SIAM J. Imag. Sci., vol. 1, no. 3, pp. 248-272, 2008.
- [21] J. Yang, Y. Zhang, and W. Yin, "An Efficient TVL1 Algorithm for Deblurring Multichannel Images Corrupted by Impulsive Noise", SIAM J. Sci. Comput., vol. 31, no. 4, pp. 2842-2865, 2009.
- [22] A. Foi, K. Dabov, V. Katkovnik, and K. Egiazarian, "Shape-Adaptive DCT for denoising and image reconstruction," *Proc. SPIE Electronic Imaging: Algorithms and Systems V*, 6064A-18, (San Jose, CA, USA), 2006.

[23] K. Dabov, A. Foi, V. Katkovnik, and K. Egiazarian, "Image restoration by sparse 3D transform-domain collaborative filtering," *Proc. SPIE Electronic Imaging*, Jan. 2008.